J Math Chem (2010) 48:424–438
DOI 10.1007/s10910-010-9684-4

ORIGINAL PAPER

On the unimolecular elimination of gas-phase iodine monobromide following excitation in the visible wavelength region

Dongfang Zhang

Received: 17 July 2009 / Accepted: 19 April 2010 / Published online: 30 April 2010

Abstract Dissociation dynamics of iodine monobromide has been theoretically investigated at numerous excitation wavelengths in the visible wavelength region (450–540 nm) by an accurate time-dependent dynamical simulation technique. The interatomic potential energy curves are derived from ab initio methods which are then employed in a Landau–Zener treatment to calculate the spin-orbit branching ratios in the two halogen products. The extinction coefficients, in arbitrary units, for the discrete electron transition are obtained through a numerical algorithm. Based on these elastic scattering calculations, the results of Br*: Br branching ratios are determined at several simulation wavelengths. Also the electronic properties are evaluated to elucidate the mechanism of chemical dynamics of the system. It is found that the branching dynamics can be clarified via the Landau–Zener model, which treats an avoided crossing between two states of a given nature and evaluates a nonadiabatic effect relevant to the dissociation of IBr molecule.

Keywords Dissociation · Elastic scattering · Chemical dynamics

1 Introduction

Unimolecular reaction, such as the transfer of angular momentum or electron following excitation between the various valence states, are at the heart of many chemical phenomena, which can be viewed as the elastic scattering and are essential to the understanding of chemical dynamics [1–16]. During the fragmentation processes, rupture or formation of chemical bonds and energy flow in molecule systems are inevitably to happen. After the birth of wave packet simulation techniques in chemistry field and

D. Zhang (✉)
College of Science, Huazhong Agricultural University, 430070 Wuhan, People's Republic of China
e-mail: zdfbb@yahoo.cn

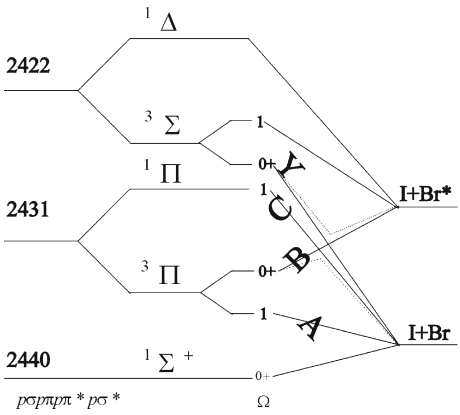

Fig. 1 Correlation diagram of iodine monobromide, and various dissociation paths

with a wealth of accumulated information concerning molecular dynamics or reaction process [17–44], many simple systems especially the interhalogen molecules have received wide attention for decades and long served as the representative systems for exploration of dissociation mechanism. A typical example is the IBr molecule, which is broadly explored for studying the electronic structure and non-adiabatic coupling phenomena in molecular dissociation. Upon absorption of a photon, the IBr molecule is excited to the valence states correlating with the different combinations of $I(^2P_J)$ and $Br(^2P_J)$ atomic products. As is shown in Fig. 1, the correlation diagram of IBr gives the information about the electronic configurations and their corresponding asymptotic limits. For convention, the main electronic states via excitation in the visible absorption continuum can be labeled as $^1\prod_1$ (two manifold), $^3\prod_1$ (two manifold), $^3\prod_{0+}$ (two manifold) and $^3\Sigma^-_{0+}$, respectively. In adiabatic picture, from which the total angular momentum quantum numbers omega, or the off-diagonal matrix elements of the electronic Hamiltonian (or the spin-orbit operator) should be taken into account, the $A^3\prod_1$, $C^1\prod_1$ and $Y^3\Sigma^-_{0+}$ states will correlate to the ground state bromine atoms, whereas the $B^3_{0+}\prod$ state generates spin-orbit excited state Br* ($^2P_{1/2}$) upon dissociation.

A series of experimental studies have been carried out to determine the dissociation channels and role of nonadiabatic effects during the course of IBr dissociation. Despite the apparent simplicity of the electronic bands, numerous curve crossings and overlapping electronic states must be invoked to explain the experimentally observed parameters of daughter atoms. It has been revealed that the probability of heterogeneous transitions ($\Delta\Omega = 1$) between the states of different symmetry is negligibly small. On the contrary, the homogeneous interaction ($\Delta\Omega = 0$) caused by the states of same symmetry is assumed to be relatively important, which leads to a strong wavelength dependence for both of the branching into ground and spin-orbit excited state Br atoms and the recoil anisotropy of the I+Br product.

In spite of the extensive investigations of the IBr molecule visible absorption system, information about the potential energy curves for the relevant excited states and chemical dynamics in the course of dissociation is far from being complete and unambiguous. Attempts to understand the effects of the nonadiabatic behavior that added to the swarm of trajectories have focused on the measurement of quantum yields for

the ground state and spin-orbit excited fragments or product anisotropy parameter. Nonetheless, the anisotropy parameter beta contains important information on photoexcitation, such as directions of the transition moment, but shows little information about the dissociation dynamics after photoexcitation, the shape of potential energy curves far from the Franck–Condon region, and so on. Moreover, since the interference effects in the orientation of the total angular momentum of the products are quite sensitive to the details of the entire dissociation processes, their theoretical simulation would provide a wealth of information about the dissociation dynamics [45–64]. We thus expect that such information may be detailed enough to resolve the previously mentioned controversy on the nonadiabatic mechanisms. Furthermore, since some experimental results are not consistent with one another, it is useful to theoretically analyze details of the experimental results.

The paper mainly describes a theoretical study of the excited state dynamics of IBr and the main result is a deconvoluted absorption spectrum and comparison of theoretical and experimental avoided crossing probabilities. It employs standard theoretical methods: time-dependent density functional theory to describe the excited states and Landau–Zener transition probability theory to describe the non-adiabatic crossing between different electronic states. The organization of this article is as follows. The second section is devoted to describe the dynamical behavior of the $j = 1/2$ of the product atom in terms of a quantum nuclear wave packets running on adiabatic potential energy surfaces determined with quantum chemical method of enough computational size. With the electronic curves the one-dimensional time dependent Schrödinger equation is solved in order to obtain data for estimation of energy dependent amplitudes and total cross sections. The third section reports the numerical results found for some valence states and a discussion of our results and their comparison with those arising from prior data are made. Finally, the last section points out the remarks and conclusions of this work.

2 Summary of theoretical aspects

The theoretical treatment is performed to solve the time-dependent Schrödinger equation for the relevant initial conditions,

$$i\hbar \frac{\partial |\Psi(\mathrm{R,t})\rangle}{\partial \mathrm{t}} = \hat{H} |\Psi(\mathrm{R,t})\rangle \tag{1}$$

where R are the coordinates of the particles. Here the Hamiltonian $\hat{H}$ is the sum of the nuclear kinetic energy operator $\hat{I}(\mathrm{R})$ plus the electronic potential energy $\hat{U}(\mathrm{R})$ and the spin-orbit Hamiltonian $\hat{H}_{so}(\mathrm{R})$. For convenience, we consider the dissociation of a diatomic molecule XY producing the fragments X and Y with angular momenta J_X and J_Y, respectively. The projection of the angular momentum J_X, J_Y onto the laboratory axis Z is m_X and m_Y, respectively.

The initial wave packets are constructed by multiplying the ground state vibrational wave function ξ_v by the appropriate transition moment functions $\chi_j(\mathrm{R})$

$$[\Psi(\mathrm{R,t}=0)] = \begin{pmatrix} \mathrm{f}_1(\mathrm{R},\mathrm{t}=0) = \chi_1(\mathrm{R})\xi_v \\ \mathrm{f}_2(\mathrm{R},\mathrm{t}=0) = \chi_2(\mathrm{R})\xi_v \\ \vdots \\ \mathrm{f}_n(\mathrm{R},\mathrm{t}=0) = \chi_n(\mathrm{R})\xi_v \end{pmatrix} \tag{2}$$

where $[\Psi(\mathrm{R,t}=0)]$ denotes an ensemble of the initial wave packet $\Psi_j(\mathrm{R},\mathrm{t}=0)$ ($j = 1, 2, \ldots, n$) formed on the jth excited state into matrix representations, $\chi_j(\mathrm{R})$ is the transition moment associate the jth excited state with the ground state.

The general solution of Eq. (1) is

$$|\Psi(\mathrm{t})\rangle = \exp(-i\hat{H}\mathrm{t}/\hbar)|\Psi(\mathrm{t}=0)\rangle \tag{3}$$

where $\exp(-\mathrm{i}\hat{H}\mathrm{t}/\hbar)$ is the time evolution operator, and used to propagate wave packet $\Psi(\mathrm{t}=0)$ on a manifold dissociative surface. The propagation scheme employs a symmetric splitting operator technique

$$|\Psi(\mathrm{R},\mathrm{t}+\mathrm{dt})\rangle = \mathrm{e}^{-i\hat{V}dt/2\hbar}\mathrm{e}^{-i\hat{I}\mathrm{dt}/\hbar}\mathrm{e}^{-i\hat{V}\mathrm{dt}/2\hbar} * |\Psi(\mathrm{R},\mathrm{t})\rangle \tag{4}$$

After each time step dt, the autocorrelation function $\Theta(\mathrm{t})$, is calculated:

$$\Theta(\mathrm{t}) = \sum_{\mathrm{j}} \int_{\mathrm{R_{min}}}^{\mathrm{R_{max}}} \langle \Psi_{\mathrm{j}}^{*}(\mathrm{R},\mathrm{t}=0)|\Psi_{\mathrm{j}}(\mathrm{R},\mathrm{t})\rangle \mathrm{dR} \tag{5}$$

The total cross-section $\rho_{\mathrm{tot}}(\nu)$ as a function of photoexcitation frequency ν is given by Fourier transformation, which can be expressed as

$$\rho_{\mathrm{tot}}(\nu) = \frac{\pi\nu}{3c\varepsilon_0\hbar} \int_{-\infty}^{\infty} \mathrm{dt}\exp[\mathrm{i}(\mathrm{E}_{\nu''} + \mathrm{h}\nu)\mathrm{t}/\hbar]\Theta(\mathrm{t}) \tag{6}$$

where ε_0 is the permittivity of vacuum and $\mathrm{E}_{\nu''}$ is the energy of the initial state for individual vibrational quantum number.

The partial cross-section of dissociation for a certain channel $\rho_j(\nu)$ is derived by collecting the information of wave packet $\Psi_j(\mathrm{R},\mathrm{t})$ at an analysis line $\mathrm{R} = \mathrm{R_f}$, in the asymptotic region, which is a function of excitation frequency ν

$$\rho_j(\nu) = \left(\frac{4\pi^3\,\nu\,k_j}{3c\,\varepsilon_0\,M}\right)\left|\Theta_j(R_f, E)\right|^2 \tag{7}$$

$$\Theta_j(R_f, E) = \frac{1}{2\pi}\int_0^\infty \Psi_j(R_f, t)\exp[i(E_{\nu''} + h\,\nu)t/\hbar]dt \tag{8}$$

where M being the reduced mass of IBr, $E_{\nu''}$ is the vibrational energy of a given ν'' level and k_j is the wave vector of fragments in channel j, which is deduced from

$$k_j = [2M(h\nu - V_j(R_f))]^{1/2}\hbar^{-1} \tag{9}$$

The total cross section in cm^2 is changed into the molar absorption coefficient by $\omega = 10N_A\rho/\ln 10$, where N_A is the Avogadro constant, $6.022 \times 10^{23}\ mol^{-1}$.

The calculations are performed using equidistant grids for the internuclear coordinate. As wave packets reach the asymptotic region, they must be attenuated by the absorbing potential to avoid boundary reflection. The coefficients of absorbing potential are

$$\vartheta_{abs}(R) = 1.0 \quad R < R_{abs} \tag{10}$$

$$\vartheta_{abs}(R) = \exp(-\gamma_{opt}\cdot dt)\left(\frac{R-R_{abs}}{R_{max}-R_{abs}}\right)^{1.5} \quad R_{abs} < R < R_{max} \tag{11}$$

where R_{abs} is the starting point of damping, γ_{opt} is an optimum factor for damping. Values of all parameters used in calculations are listed in Table 1. The computations of electronic structure and simulations of nuclear motion are performed by using computer code of FORTRAN language. In the calculations, the occupied orbital space is divided into a set of inactive or closed-shell orbitals and a set of active orbitals. All inactive orbitals are doubly occupied in each Slater determinant. On the other hand, the active orbitals have varying occupations, and all possible Slater determinants (or CSFs) are taken into account which can be generated by distributing the $N_{act} = N_{el} - 2m_{closed}$ electrons in all possible ways among the active orbitals, where m_{closed} is the number of closed-shell (inactive) orbitals, and N_{el} is the total number of electrons. Thus, it corresponds to a full CI in the active space. On this basis, the relevant 14 electrons are set as active, and the orbital inspection are carried out by RHF/STO-3G method. Practical active spaces increase to about 10 orbital for energies and gradients, which involving the valence orbital and their correlation with nonvalence orbital. The relativistic ab initio model potential (AIMP) effective core potentials (ECP) are used for I or Br, which are contracted to (7s, 6p, 4d, 3f, 2g) and (6s, 5p, 3d, 2f, 1g), respectively.

3 Results and discussion

Figure 2 shows the calculated electronic potential curves as a function of nuclear distance of R. These curves are roughly categorized into two types of diabatic curves.

Table 1 Input parameters used to perform the wave packet calculations

Parameters	Classification	Magnitude
Atomic masses	M_{I}	126.90447 amu
	M_{Br}	79.904 amu
Reduced masses	M	49.03172 amu
Range of grid	R_{min}, R_{max}	3.78–17.0 a_0
Number of grid points	n_1	4096
Time step	dt	0.483776 fs
Number of time steps	n_2	8192
Start of absorbing region	R_{abs}	15.12 a_0
Amortization factor	γ_{opt}	0.015 fs^{-1}

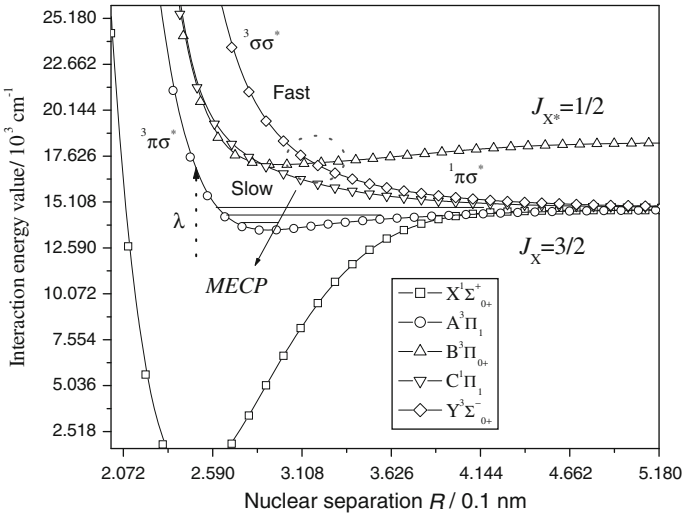

Fig. 2 The interaction potentials of iodine monobromide along the Br–I bond elongation coordinate at linear geometry, and various dissociation channels

The first kind is those having a somewhat deep potential walls or having bound properties. The second type simply belongs to the repulsive curves. Among them, the $A^3\prod_1(\Omega=1)$, $C^1\prod_u(\Omega=1)$ and $Y^3\Sigma^-(\Omega=0)$ states asymptotically correlate to the ground state $Br(j=3/2)+I$ limit, whereas the $B^3\prod(\Omega=0)$ state correlates with the excited state $Br^*(j=1/2)+I$ dissociation limit. Of course, the diabatic curves correlating to final products split into two at large R. This splitting is mainly responsible for the atom exchange process. In the region of $E\approx 0.0786$ hartree and $R\approx 0.3177$ nm, a minimal energy crossing point is existed, which results in a coupling of the quasi-bounding B state with the repulsive states Y. The effect originates from the intersecting located between the two involved adiabatic potential curves. In the interaction region where the excited and ground states become degenerate, the nonradiative transition can ultimately convert the photon energy into a nonstatistical

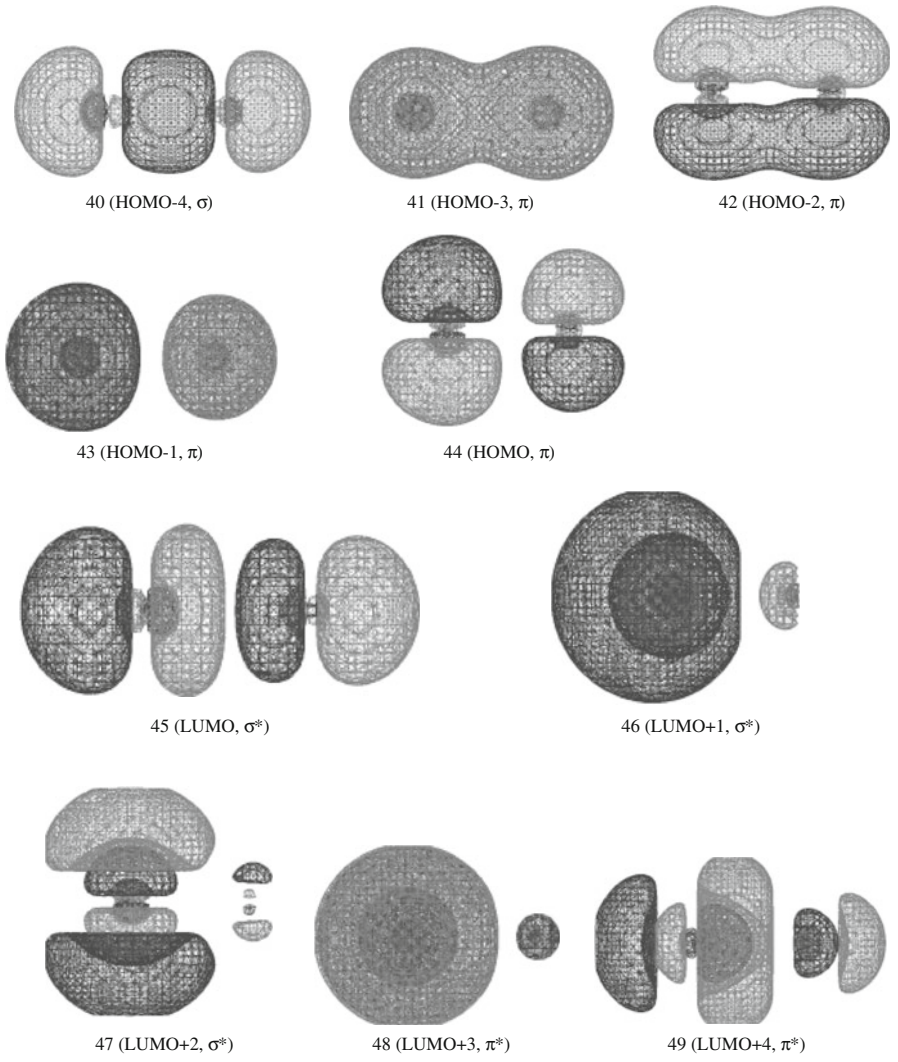

Fig. 3 A schematic diagram showing the structure of the highest doubly occupied molecular orbitals and the lowest unoccupied orbitals

distribution of quantum flux. Due to the similar symmetry ($\Omega = 0^+$ and 0^-) of B and Y electronic states, the avoided crossing is naturally formed between them. As will be discussed below, the avoided crossing plays a very important role in electronically nonadiabatic transitions. In Fig. 3, we show the relevant molecular orbitals that participate in the course of dissociation, which correlate to the low lying excited states of IBr and contain the five highest occupied molecular orbitals (HOMO) and the five lowest unoccupied orbitals (LUMO) with their related bonding nature. The positions of iodine and bromine nuclei are indicated as bond direction, which is defined as Z-axis for the convenience of marking the p orbital. The MOs considered here are those that are rel-

Table 2 The electric dipole moments μ_0 (in atomic units; $1ea_0 = 2.54158$ debye), corresponding main excitations and oscillator strengths f, for the IBr molecule in the equilibrium geometry

Spin free states	Leading transitions	Dipole moments μ_0 (ea_0)	λ_{ex}/nm	Osc. strength & CI. coefficient
$^3\Pi(\Omega = 1)$	43, 44 to >45; $\pi\sigma^*$	0.60	574.98	f = 0.0001, 0.80440
$^3\Pi(\Omega = 0)$	41, 42 to >45; $\pi\sigma^*$	1.61	448.451	f = 0.0001, 0.74548
$^1\Pi(\Omega = 1)$	41, 42 to >45; $\pi\sigma^*$	1.22	434.556	f = 0.0014, 0.66904
$^3\Sigma(\Omega = 0)$	40 to >45; $\sigma\sigma^*$	0.0	298.528	f = 0.0004, 0.82554

evant in I–Br cleavage of the IBr molecule. Apparently in the picture, the p lone-pair orbital of the atoms, which are the five energetically highest occupied MOs, become the main source for the formation of the low-lying excited states. Table 2 summarizes the low-lying excitations of the parent IBr molecule. According to the computations, in both states, the transition from HOMO to LUMO (40 to >45) calculated at 4.152 eV (298.528 nm) and transition (41, 42 to >45) calculated at 2.853 eV (434.556 nm) are found to dominate the absorption from the estimated oscillator strength $f = 0.0004$ and $f = 0.0014$, respectively. Because the excitation energies for the 40 to >45 transition lies very close to the Rydberg transition, the visible spectrum band can be ascribed largely to the transitions to the first lowest unoccupied molecular orbital, namely, the front virtual orbital. The Orbital energies obtained for the two highest occupied molecular orbital are both -0.2846 hartree, while the front LUMO has orbital energy of -0.1805 hartree. Therefore, the photon energy required for excitation is about 2.833 eV (437.678 nm) and transition to $C^1\Pi_1$ state can be achieved. This indicates that absorption profile will show a maximum coefficient nearby the wavelength of 440 nm, which accords with the above dynamical prediction that extinction intensity will reach its peak value of 449 nm and most experimental results.

Figure 4 shows the the absorption spectrum calculated using the exact propagation method. The involved principle is that the light absorption promotes the reactant molecule to an excited electronic state that is associated with a different PES. In fact, the reactant is vertically excited into the excited electronic state [Franck–Condon (FC)] principle creating a population far from thermal equilibrium. Recasting this qualitative picture in the theoretical framework of quantum dynamics, the initial excitation will prepare a nonstationary nuclear wavepacket (WP). The time-evolution of the WP has an approximate classical representation in terms of a set of trajectories released on the excited state PES whose initial positions and velocities "sample" the probability density of the quantum state. In this context, the transition mechanism is assumed to involve the absorption of a single photon of visible radiation which causes the molecule transforming from a bound to a dissociative electronic state. As is shown, the computed results of the partial absorption coefficient ρ (unit:mole^{-1}l·cm^{-1}) to the A, B, and C states reflecting their relative weight in the initial population. Also portrayed are the total absorption coefficients from these discrete states, which corresponding to the schematic convolution of the partial absorption spectrum and indicate that the A–X and, particularly, B–X transitions contribute to the continuous absorption at shorter wavelengths ($\lambda < 505$ nm). For comparison, gas phase spectrum of IBr recorded over

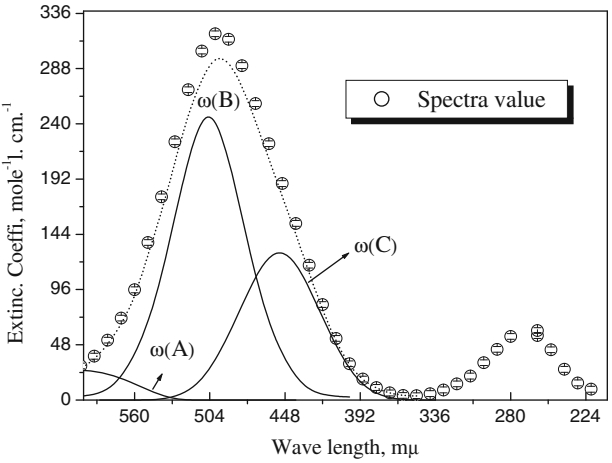

Fig. 4 Correlation between the photolysis wavelengths and the extinction coefficients. *Open hexagon* experimental data from Ref. 65; *dotted* and *solid lines* numerical predictions

the wavelength range 220–600 nm (hexagon symbol) of Daniel et al. [65] is referred to in the graph. It can be seen that the general shape and intensity of computation closely resemble that actually observed with the path length employed, there are only slight deviations in the magnitude of total coefficient near the intermediate region (480–520 nm) of the this visible spectrum band. Thus the method, even if approximate, has proven to be reliable enough to give good estimates of the absorption maximum and the mid-height width of the spectrum, as well as a correct range for the evolution of the geometry during the dissociation timescale with respect to accurate propagation methods. Here the photoexcitation to the higher $Y^3\Sigma^-_{0+}$ state requires much more energy ($\sim$4.152 eV, shown in Table 2) in the Franck–Condon region, which is unable to be accomplished directly via visible photon. Thus, initial excitation to the $Y^3\Sigma^-_{0+}$ state is ignored in our simulation.

On the basis of the model as introduced above, the dynamics in different coupled electronic states can be described. In the following, the nonadiabatic dynamics will be clarified by calculating the branching dynamics semiclassically directly. In a diabatic picture, the wave packet starts to propagate on the potential curve of the electronic B state after the excitation of the molecule into its B state. The interaction with other states can induce the B state predissociation, which is viewed as an outcome of an interaction between the repulsive Y and the bound B state potentials in the neighborhood of their crossing point on the outer limb of the B state well. There are two different channels involved: the $B^3\prod(\Omega = 0^+)$ as well as the $Y^3\Sigma^-(\Omega = 0^+)$ state. Predissociation via the Y state can not be neglected due to the nature of the interference process makes it most salient in systems of coupled potential energy surfaces at intermediate coupling strength. Given the appropriate dynamical circumstances in a fully coupled system hybrid diabatic–adiabatic wave packet trajectories will become important. Therefore, the dynamical calculations should provide a means to examine the quantum interference, which may happen at potential energy curve crossings

and the created wave packet fractions thereafter propagate independently along an adiabatic or a diabatic path, separately. If considered using the adiabatic representation, these two states both possess the same 0^+ symmetry and an avoided crossing effect will born in the region of strong configuration mixing (as shown in Fig. 1). Usually, the mixing can not simply explained in either a full adiabatic or diabatic pattern, thus it is valuable to using a semiclassical model treats an avoided crossing between two states of a given nature and evaluates a nonadiabatic transition. In linear iodine monobromide, the formation of Br at all dissociative wavelengths employed in this work is generally explained by invoking the well-known one-dimensional curve crossing model between B and Y states. The model combines the soft radical model for energy disposal with the one-dimensional Landau–Zener description of the curve crossing probability. Given the foregoing analysis of the wavelength dependence of the branching ratio and beta parameter for the Br + I products arising in IBr photolysis at visible absorption range, the determination of in which cases quantum interference effects should be taken into account. Since the B state is the only electronic with 0^+ symmetry that can be achieved through a $\Delta\Omega = 0$ vertical excitation from the X state, thus the previous measurement that a lot of parallel contribution to the Br + I products formed reflects the key role of the interplay between the diabatic B and Y potentials at stretched bond distance. The probability for the predissociation can be computed using the Landau–Zener formula. The probability θ for flux transfer from B to Y after passing through their crossing, which can be viewed as flux remaining on one of the diabatic potentials (Y state) is given by

$$\theta = 1 - \exp\left[\frac{-2\pi|\mathrm{W}_{12}|^2}{\hbar|\mathrm{V}_1' - \mathrm{V}_2'|u_r(\mathrm{b})}\right] \tag{12}$$

where, W_{12} is the coupling term between the two adiabatic potentials, $\mathrm{V}_\mathrm{i} = \mathrm{dV_i/dx}$ is the derivative or gradient of the potential $\mathrm{V_i}$ with respect to the intermolecular distance coordinate x at the crossing point and u is velocity of the molecule at this point. The relative radial velocity u is a function of the impact parameter b, and the probability of surface hopping is related to θ by Eq. (12); hence, θ is also a function of b (which group the characteristic of potentials together, $\mathrm{b} = \{4\pi^2|\mathrm{W}_{12}|^2/\mathrm{h}|\Delta\mathrm{V}|\}$), whereas b is also adjustable since its magnitude relies much on the splitting between adiabatic surfaces.

In this work, the coupling strength $\mathrm{V_{B/Y}}$ is assumed to taken a series of empirical values from 80 to 180 cm^{-1} and its application in the Landau–Zener model can provide a quantitative understanding of the nonadiabatic dynamics. As shown in Fig. 5, the probability for the flux that initially excited to the B state and then follows the adiabatic pathway and switching to the diabatic Y surface to generate atomic Br have a practical trend to decline with the decreasing photolysis energy. Since the energy of the avoided crossing is located far from the exit channel, as a consequence, the radial velocity at the point of crossing is relatively sensitive to the photolysis wavelengths, which in turn influence the probability of crossing. Still we can note that the probability decreases approximately linearly with the increasing coupling strength $\mathrm{V_{B/Y}}$, this because part of the wave packet ejected from the diabatic B state will be difficult to be attracted to the Y state when passing the crossing due to the coupling force coming from the

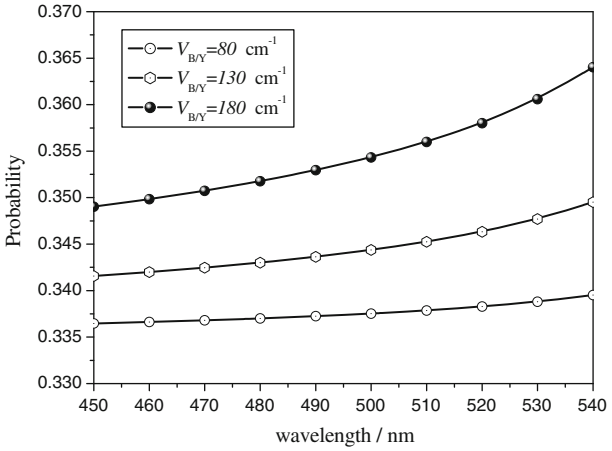

Fig. 5 Correlation between the photolysis wavelengths and the nonadiabatic transition probability, which are obtained at the case of different coupling strength

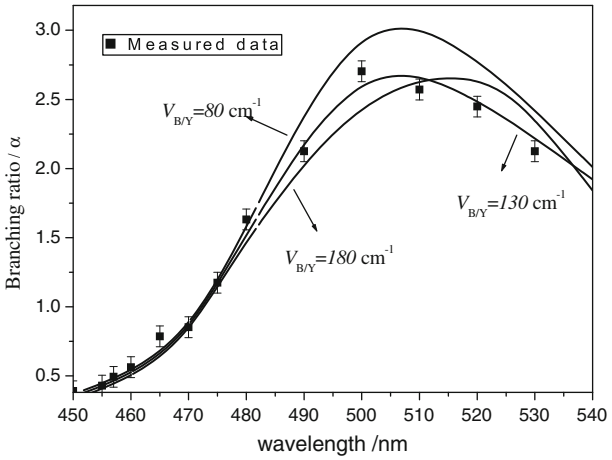

Fig. 6 Comparison of experimentally measured branching ratios with the theoretical values. The coupling strength between the B and Y states is adjusted from 80–180 cm^{-1}

interaction between the above two states. When the dissociation event is finished, the branching ratio α of the Br* relative to the Br fragments should be determined by two factors: the state population and transition probability, which can be readily inferred by the following equations,

$$\alpha(\mathrm{Br}^* : \mathrm{Br}) = \frac{\omega(B^3\Pi_{0+})(1-\theta)}{\omega(A^3\Pi_1) + \omega(C^1\Pi_1) + \omega(B^3\Pi_{0+})\theta} \tag{13}$$

where ω is the extinction coefficients for the electronic transitions.

As is shown in Fig. 6, the simulation accords well with the experimentally obtained branching feature of the $Br(^2P_J)$ formation channel when the coupling parameter $V_{B/Y}$

is fixed as 130 cm^{-1}. This indicates although the ground Br atoms mostly come from the A and C states, from which the initial excitation involves a $\Delta\Omega = 1$ transition, the Y state can also contribute the formation of $Br(^2P_{3/2})$ products. Since the coupling strength is intermediate, part of the flux evolving along the B state surface will transferred to the Y state potential and following the adiabatic route. The above effects can change the flux distribution between two different exit channels. Only if the coupling strength is large, the flux will have to remaining on the B state surface and not reach to the I+Br dissociate limit, which is essential in the interaction case. According to the Landau–Zener theory [66], the nonadiabatic surface transition probability should be small when these two surfaces are almost parallel to each other. That might explain why the obtained branching ratio for the numbers of Br*: Br products are somewhat larger than the adiabatic case, because the triplet–triplet coupling strength is not weak from the topology of these two potentials (B and Y state). Moreover, considering the expression of the asymmetry parameter Q [67]:

$$Q = 2\frac{1+\varpi^2\tau^2}{1+4\varpi^2\tau^2}P_2\cos(\varphi) \tag{14}$$

where ϖ is the angular velocity of the parent molecule, τ is the dissociation lifetime, and φ is the angle between the transition moment and the direction of the fragment. If the dissociation process is much shorter than the rotational period of the molecule, that is, $\varpi\tau \ll 2\pi$ the expression become

$$Q \simeq 2P_2\cos(\varphi) = 3\cos^2\varphi - 1 \tag{15}$$

Then the asymmetry parameter Q of Br channel is estimated to be ~ -1.0 at 520 nm, which is much different from the experiment value of 1.20, confirming that the dissociation is not a direct process. In view of the interaction of avoided-crossing, the Br channel may originate from two components: direct excitation of the A and C states and the B $\rightarrow$ Y nonadiabatic transition. The direct contribution in the Br channel is considered to have a perpendicular character ($\beta = -1$), while the nonadiabatic contribution remains the same anisotropy as the fragments that appear in the Br* channel [β(Br*)$= +2$]. Therefore, the β(Br) value may be resolved to the relative contributions of the parallel and perpendicular components (Eq. (16))

$$\beta = a\beta_{\parallel} + b\beta_{\perp} = a\beta(\mathrm{Br}^*) + b(-1) \tag{16}$$

Here, a and b denote the fractions of nonadiabatic and direct excitation contributions in the Br product channel. The former fraction is determined by Eq. (17).

$$a = \frac{1+\beta(\mathrm{Br})}{1+\beta(\mathrm{Br}^*)} \tag{17}$$

Provided that β(Br) and β(Br*) are given along with the application of $a + b = 1$. The avoided-crossing probability P between the B and Y states is expressed as Eq. (18).

$$P = \frac{a\Phi(\mathrm{Br})}{\Phi(\mathrm{Br}^*) + a\Phi(\mathrm{Br})} \tag{18}$$

where Φ represents the relative quantum yields of final products. With the experimental data of β(Br), β(Br*), Φ(Br) and Φ(Br*), the P value is therefore evaluated to be 0.30. It means about 30% quantum flux arising from B state will channeled into the Br channel during the fragmentation process. The results suggest that the photochemical dynamics of IBr molecule upon excitation within the visible region is rightly dominated by the avoided crossing mechanism, which can be explained by employing the Landau–Zener model. If the crossing point is located at a significantly higher energy, a dramatic change in the crossing probability would be expected [68]. The superfluous formation of Br* in most simulation wavelength region hints the coupling strength between B and Y states plays an important role in dissociation course.

4 Conclusion

This manuscript is concerned with the electronic transitions and dissociation of IBr molecule. Branching dynamics of $\mathrm{Br}(^2\mathrm{P_J})$ products in the fragmentation of molecular IBr following excitation in the visible absorption band has been investigated via the wave packet simulation on nuclear motion on various excited surfaces. The nonadiabatic probabilities are estimated as a function of different wavelengths by using the classical Landau–Zener theory. Based on these results and the properties of the relevant molecular orbitals (actually determined with the time-dependent DFT), the pertinent mechanism of transitions are discussed. The calculated extinction intensity and quantum yields for $j = 1/2$ of the product Br atom shows a good agreement with the experimental values, and serves to validate that the dissociation dynamics follows the one-dimensional Landau–Zener curve crossing model generally. The best fitting value of coupling parameter $V_{B/Y}$ between the B and Y states is determined to be about $130\,\mathrm{cm}^{-1}$, which agrees with experimental results in the most energy range. The coupling force is found to have a significant impact on the observed branching dynamics.

Acknowledgment This work was supported by Huazhong Agricultural University Scientific & Technological Self-innovation Foundation (2009QC016).

References

1. S.A. Vazquez, E. Martinez-Nunez, Chem. Phys. **349**, 219 (2008)
2. J. Pittner, H. Lischka, M. Barbatti, Chem. Phys. **356**, 147 (2009)
3. G. Rojas-Lorenzo, J. Rubayo-Soneira, S.F. Alberti, Chem. Phys. **362**, 34 (2009)
4. G.E. Douberly, R.E. Miller, Chem. Phys. **361**, 118 (2009)
5. T.R. Rao, B.J. Rao, S. Mahapatra, Chem. Phys. **365**, 129 (2009)
6. Q. Meng, J. Zhao, Y. Xu, D. Yue, Chem. Phys. **362**, 65 (2009)
7. H. Koppel, B. Schubert, H. Lischka, Chem. Phys. **343**, 319 (2009)

8. B.I. Loukhovitski, A.M. Starik, Chem. Phys. **360**, 18 (2009)
9. J.P. Malhado, J.T. Hynes, Chem. Phys. **347**, 39 (2008)
10. A. Borowski, O. Kuhn, Chem. Phys. **347**, 523 (2008)
11. J. Friedrichs, K. Damianos, I. Frank, Chem. Phys. **347**, 17 (2008)
12. I. Antol, M. Vazdar, M. Barbatti, M. Eckert-Maksic, Chem. Phys. **349**, 308 (2008)
13. R. Schinke, S.Y. Grebenshchikov, H. Zhu, Chem. Phys. **346**, 99 (2008)
14. D.P. Hydutsky, N.J. Bianco, A.W. Castleman Jr, Chem. Phys. **350**, 212 (2008)
15. I. Frank, K. Damianos, Chem. Phys. **343**, 347 (2008)
16. R. Vetter, Chem. Phys. **343**, 303 (2008)
17. Y. Zhang, J.E. Straub, J. Chem. Phys. **130**, 095102 (2009)
18. C. Berkdemir, J. Math. Chem. **46**, 139 (2009)
19. B.K. Dey, P.W. Ayers, J. Math. Chem. **45**, 981 (2009)
20. S.W. Zhang, D.J. Tan, J. Math. Chem. **44**, 217 (2008)
21. Y.A. Pisarenko, Russ. J. Phys. Chem. A. **82**, 1 (2008)
22. V.A. Durov, I.Y. Shilov, Russ. J. Phys. Chem. A. **82**, 83 (2008)
23. V.I. Deineka, Russ. J. Phys. Chem. A. **82**, 108 (2008)
24. E.D. Totchasov, G.A. Alper, Russ. J. Phys. Chem. A. **82**, 71 (2008)
25. M.A. Margulis, Russ. J. Phys. Chem. A. **82**, 122 (2008)
26. A.A. Čučulović, D. Veselinović, S.S. Miljanić, Russ. J. Phys. Chem. A. **83**, 1547 (2009)
27. K.S. Gavrichev, M.A. Ryumin, A.V. Tyurin, V.M. Gurevich, L.N. Komissarova, A.V. Khoroshilov, G.A. Sharpataya, Russ. J. Phys. Chem. A. **83**, 327 (2009)
28. O.S. Subbotin, V.R. Belosludov, E.N. Brodskaya, E.M. Piotrovskaya, V.V. Sizov, Russ. J. Phys. Chem. A. **82**, 1303 (2008)
29. S.G. Dyakonov, A.V. Klinov, G.S. Dyakonov, Russ. J. Phys. Chem. A. **83**, 875 (2009)
30. M.F. Butman, V.B. Motalov, L.S. Kudin, A.E. Grishin, A.S. Kryuchkov, K.W. Krämer, Russ. J. Phys. Chem. A. **82**, 164 (2008)
31. D.N. Putintsev, N.M. Putintsev, Russ. J. Phys. Chem. A. **83**, 265 (2009)
32. G.N. Sargsyan, Russ. J. Phys. Chem. A. **83**, 1712 (2009)
33. D. Zhang, Polish J. Chem. **83**, 2009 (2009)
34. V.A. Durov, A.P. Moscalets, Russ. J. Phys. Chem. A. **83**, 990 (2009)
35. D.K. Belashchenko, O.I. Ostrovskii, Russ. J. Phys. Chem. A. **82**, 364 (2008)
36. V.I. Bykov, S.B. Tsybenova, Russ. J. Phys. Chem. A. **83**, 609 (2009)
37. G. Gao, S.H. Park, H.S. Kang, Chem. Phys. **355**, 50 (2009)
38. G. Pierdominici-Sottile, J. Palma, Chem. Phys. **363**, 59 (2009)
39. S. Mishra, R.K. Singh, A.K. Ojha, Chem. Phys. **355**, 14 (2009)
40. G. Grigorian, A. Cenian, Chem. Phys. **359**, 31 (2009)
41. M.E. Beck, M. Schindler, Chem. Phys. **356**, 121 (2009)
42. S. Jorgensen, A. Gross, Chem. Phys. **362**, 8 (2009)
43. M. Nsangou, M.L. Senent, M. Hochlaf, Chem. Phys. **355**, 164 (2009)
44. B. Dietzek, A.N. Tarnovsky, A. Yartsev, Chem. Phys. **357**, 54 (2009)
45. D. Zhang, Chem. Phys. **353**, 87 (2008)
46. M.J.J. Vrakking, D.M. Villeneuve, A. Stolow, J. Chem. Phys. **105**, 5647 (1996)
47. D. Zhang, J. Math. Chem. **46**, 576 (2009)
48. G.E. Busch, R.T. Mahoney, R.I. Morse, K.R. Wilson, J. Chem. Phys. **51**, 837 (1969)
49. D. Zhang, A. Abdel-Hafiez, B. Zhang, Chem. Phys. Lett. **428**, 49 (2006)
50. D. Zhang, A. Abdel-Hafiez, B. Zhang, Chem. Phys. **342**, 119 (2007)
51. D. Zhang, A. Abdel-Hafiez, B. Zhang, Chin. J. Chem. Phys. **21**, 12 (2008)
52. D. Zhang, Russ. J. Phys. Chem. A. **82**, 2299 (2008)
53. H. Bony, M. Shapiro, A. Yogev, Chem. Phys. Lett. **107**, 603 (1984)
54. R.L. Pastel, G.D. Hagard, H.C. Miller, S.R. Leone, Chem. Phys. Lett. **183**, 565 (1994)
55. R.L. Pastel, J.K. McIver, H.C. Miller, G.D. Hager, J. Chem. Phys. **100**, 3624 (1994)
56. D. Zhang, J. Math. Chem. **47**, 29 (2010)
57. Y.S. Kim, Y.J. Jung, K.H. Jung, J. Chem. Phys. **107**, 3805 (1997)
58. L. Zhang, H. Sun, Chin. J. Chem. Phys. **22**, 69 (2009)
59. G. Jeung, Chin. J. Chem. Phys. **22**, 187 (2009)
60. R. Zhang, X. Li, X. Zhang, Chin. J. Chem. Phys. **22**, 235 (2009)
61. T. Zhang, N. Zheng, Chin. J. Chem. Phys. **22**, 246 (2009)

62. R. Zhang, Z. Tan, S. Luo, Chin. J. Chem. Phys. **21**, 221 (2008)
63. X. Zhang, M. Li, S. Tian, Chin. J. Chem. Phys. **21**, 255 (2008)
64. L. Zhang, H. Guo, Y. Pan, F. Qi, Chin. J. Chem. Phys. **21**, 547 (2008)
65. D.J. Seery, D. Britton, J. Phys. Chem. **68**, 2263 (1964)
66. E.E. Nikitin, *Theory of Elementary Atomic and Molecular Processes in Gases* (Oxford University Press, New York, 1974), p. 107
67. S. Yang, R. Bersohn, J. Chem. Phys. **61**, 4400 (1974)
68. D. Zhang, Polish J. Chem. **83**, 153 (2009)